



# Flame retardancy, thermal decomposition and mechanical properties of epoxy resin modified with copper N, N'-piperazine (bismethylene phosphonate)

Wenduo Wang<sup>1</sup> · Zhengzhou Wang<sup>1,2</sup>

Received: 18 August 2020 / Accepted: 14 January 2021 / Published online: 6 February 2021  
© Akadémiai Kiadó, Budapest, Hungary 2021

## Abstract

A metal–organic phosphonate, i.e., copper N, N'-piperazine (bismethylene phosphonate) (CuPB) was synthesized and utilized to modify epoxy resin (EP). The flame retardancy, thermal decomposition and mechanical properties of EP/CuPB composites are overall evaluated, and the mechanism is tentatively discussed. The results reveal that EP containing 3.0 wt% CuPB (EP/CuPB-3) passes UL-94 V-0 grade with an increased limiting oxygen index of 28.5%. The peak heat release rate, total heat release, total smoke release and peak CO production rate of EP/CuPB-3 in cone calorimeter test are, respectively, reduced by 43.5%, 28.0%, 37.3% and 51.9%, compared to that of pure EP. Besides, a decreased mass-loss rate ( $16.2\% \text{ min}^{-1}$ ) and an increased char yield (26.8%) of EP/CuPB-3 in the thermogravimetric analysis are achieved as a result of the char-promotion function of CuPB. Satisfactorily, the thermal resistance of EP/CuPB composites is slightly improved with an increased glass transition temperature, and the mechanical properties including tensile and impact strengths are not much affected.

**Keywords** Epoxy resin · Flame retardancy · Mechanical properties · Metal–organic phosphonates · Thermal decomposition

## Introduction

EP has been applied in fields due to the attractive properties such as adhesion, toughness and heat resistance. However, it has been of great concern that the flammability and smoke release in the combustion of EP restrict its applications to some extent [1–5]. Nowadays, the worldwide consideration of green ecosystem and sustainable development impose restrictions on the use of flame retardants containing halogen, regarding their harms to global health and ecological environment. Therefore, halogen-free flame retardants are much preferred to be exploited, especially in the electronic and electrical areas [6, 7].

Various halogen-free compounds (e.g., phosphorous, phosphorous and nitrogenous compounds, etc.) used to

flame retard EP have been investigated [8–10]. 9,10-Dihydro-9-oxa-10-phosphaphenanthrene-10-oxide (DOPO) and its derivatives as phosphorous additives [11], DOPO-based epoxy monomers [12, 13] and DOPO-based curing agents [14] have been extensively applied to flame retard EP. However, the introduction of DOPO or DOPO-based flame retardants to EP usually results in a decreased glass transition temperature ( $T_g$ ). For example, it was reported that the limiting oxygen index (LOI) of EP composite with 9.1 mass% DOPO was raised from 23.0% up to 29.0%, but the composite failed UL-94 test as well as the  $T_g$  was decreased by 24 °C and 31 °C in differential scanning calorimeter test and dynamic mechanical analysis, respectively [15]. Chi et al. designed a DOPO-based epoxy resin cured with 4,4'-diamino diphenylmethane (TEBA-DDM). The results found that the LOI of composite TEBA-DDM was increased from 25.8% to 42.3%, but the  $T_g$  was decreased from 165 °C to 136 °C, respectively, compared to the ones of untreated resin [16]. Phosphorus/nitrogen (P/N)-containing compounds are arousing increasing interests because of the synergism on flame retardance by working in the flame and promoting the carbonization, respectively, in gas and condense phases [17–19]. As one traditional P/N-containing additive, it was demonstrated that 15 mass% ammonium

✉ Zhengzhou Wang  
zwang@tongji.edu.cn

<sup>1</sup> Department of Polymeric Materials, School of Materials Science and Engineering, Tongji University, Shanghai 201804, China

<sup>2</sup> Key Laboratory of Advanced Civil Engineering Materials (Tongji University), Ministry of Education, Shanghai 201804, China

polyphosphate (APP) had endowed EP with an increased LOI value to 32.0%, relative to the value of pure EP (19.6%). Nevertheless, the strong hydrophilicity and moisture sensitivity of APP limits its applications to some extent [20, 21]. Liu et al. composed P/N-containing dimelamine pyrophosphate (DMPY) to flame retard EP. Compared to untreated EP, the incorporation of 9.0 mass% DMPY into EP obtained UL-94 V-0 grade, as well as an excellent water resistance. However, the flexural and impact strengths of this flame retarded sample were reduced by 14.4% and 15.8%, respectively [22]. Sun et al. synthesized poly (pentaerythritol phosphate phosphinic acyl piperazine) (PPAP) and found that EP with 20.0 mass% PPAP obtained a LOI value of 35.0% and UL-94 V-0 grade, as well as a 15% increase on  $T_g$  [23]. Nevertheless, high dosages of these additives usually deteriorate the mechanical performances of polymers. Herein, flame retardants with high flame retardancy and less influence on mechanical performances of polymers should be put on priority.

Metal–organic phosphonates have gained some focus as flame retardants because most of them have water insolubility and good compatibility with polymer matrix [24–26]. Moreover, it was reported that organic phosphonates were good at catalyzing the charring process of polymers during their combustions, and metallic compounds are beneficial to further enhancing and the quality of the char [27]. Wang et al. synthesized a metal–organic phosphonate, aluminum poly-hexamethylenephosphinate (APHP), to flame retard EP. The results confirmed that the LOI of EP/APHP composite was raised to 32.7% after the introduction of 4.0 mass% APHP, and a UL-94 V-1 grade was observed [28]. Ma et al. synthesized a novel metal–organic framework (Sn-MOF@PANI) to assess the fire safety performance on EP. In comparison with pure EP, 2.0 mass% Sn-MOF@PANI, respectively, resulted in a 42.0% and 32.0% reduction on peak heat release rate and total heat release of the flame retarded EP composite [29]. However, the  $T_g$  of the EP/Sn-MOF@PANI composites was slightly decreased. Phenylphosphonates were confirmed to be helpful to flame retard polymers. Wang' group fabricated a series of metal phenylphosphonates (CoPP, NiPP, CuPP and FePP), and simultaneously improvements on the thermal stabilities and flame retardancy of the flame retarded PS composites were achieved by the introduction of 2.0 mass% phenylphosphonates [30]. It was also reported that the flame retarded EP composite achieved UL-94 V-0 grade with the containing of 5.0 mass% zirconium phenylphosphonate (ZrPP), but  $T_g$  declined by about 10 °C [31]. In our recent work, a nano metal–organic phosphonate, zinc amino-tris-(methylenephosphonate) (Zn-AMP) was synthesized and applied to modify EP. It was found that EP containing 2.0 mass% Zn-AMP had much lower heat and smoke release but failed the UL-94 test and also found that the  $T_g$  of flame retarded EP composites

was not obviously influenced [32]. Generally, all these metal–organic phosphonates mentioned above are difficult in integrating good flame retardancy and thermal–mechanical performances (e.g., not reduction of  $T_g$ ) of the flame retarded EP composites at the same time. Therefore, the investigations on metal–organic phosphonates modified EP materials with well-balanced flame retardancy and thermal–mechanical properties should be of great significance.

Herein, a P/N-containing metal–organic flame retardant, copper N, N'-piperazine (bismethylene phosphonate) (CuPB), was synthesized and utilized to modify EP. The flame retardancy, thermal decomposition and mechanical properties of modified EP composites were thoroughly studied, and the flame-retardant mechanism of CuPB was tentatively illustrated.

## Experimental

### Materials

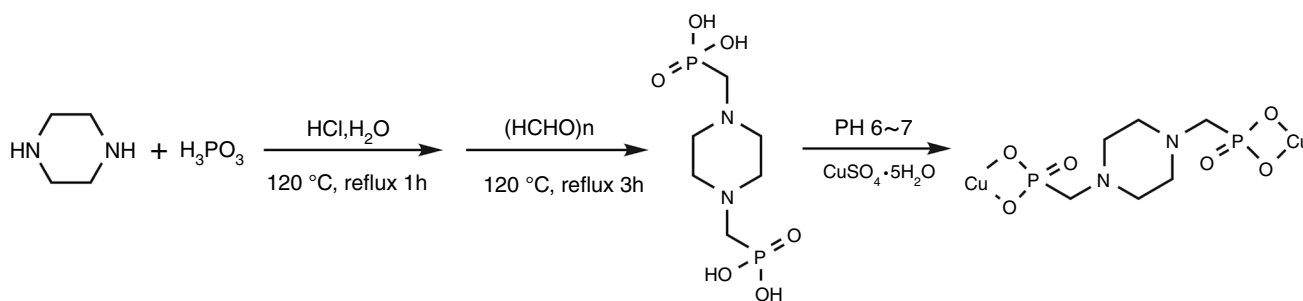
Paraformaldehyde (PFA), piperazine, copper sulfate pentahydrate, sodium hydroxide, phosphorous, hydrochloric and sulfuric acids were purchased from Shanghai Sinopharm Chemical Reagent. Bisphenol-A epoxy resin (E51) was purchased from China Sinopec Group. Curing agent 4, 4'-diaminodiphenyl sulfone (DDS) was commercially available from Shanghai Energy Chemical Reagent.

### Synthesis of CuPB

As depicted in Scheme 1, N, N'-Piperazine (bismethylene phosphonic acid) (PBA) was primarily synthesized according to Mannich method [33]: A certain of piperazine, phosphorous and hydrochloric acids (37%) were mixed in deionized water, followed by reflux under mechanical stirring. Afterwards, PFA was dropwise added to solve in the mixture. A few hours later, PBA powders were obtained. PBA (0.01 mol) was dissolved in sodium hydroxide solution, and the pH value was controlled at 6–7 by sulfuric acid. Then the solution was under mechanical stirring at room temperature for 30 min, followed by dropwise addition of a solution consisting of 0.02 mol copper sulfate pentahydrate. Subsequently, a blue turbid mixture was obtained after another 2 h stirring. Finally, CuPB was centrifugated, washed and dried. The density of CuPB was  $1.75 \pm 0.03 \text{ g cm}^{-3}$ , measured by the drainage method.

### Sample preparation

A certain epoxy resin and CuPB were stirring at 130 °C, followed by the incorporation of DDS. After DDS was dissolved, the mixture was degassed in a vacuum oven and



**Scheme 1** Synthetic route of CuPB

**Table 1** Formulations of EP and EP/CuPB composites

Samples	DGEBA/mass%	DDS/mass%	CuPB/mass%
EP	75.2	24.8	0
EP/CuPB-1	74.4	24.6	1.0
EP/CuPB-2	73.7	24.3	2.0
EP/CuPB-3	72.9	24.1	3.0

transferred to the molds to undergo a thermal curing treatment at 150 °C for 2 h and 180 °C for 4 h. Table 1 gives the formulations of the flame retarded EP composites.

## Characterization

Transmission electron microscopy (TEM) test was conducted by a JEOL JEM 2011 apparatus (Japan). X-ray photoelectron spectroscopy (XPS) was carried out by a Thermo Scientific spectrometer (USA) with an X-ray of 1484.6 eV. Fourier transform infrared spectroscopy (FTIR) were performed by using a Bruker Hyperion 2000 spectrometer (Germany). X-ray diffraction (XRD) test was performed at a scan speed of 5° min<sup>-1</sup> on a DX-1000 instrument (Fangyuan Co., Ltd., China). Scanning electron microscope (SEM) and energy-dispersive X-ray spectrometer (SEM-EDS) was performed by a Hitachi S-2360 N device (Japan). Raman was conducted in a HORIBA LabRAM instrument (Germany) (532 nm argon laser line).

LOI test was conducted by a Jiangning HC-2 instrument (China) according to GB/T2406-2009, and the specimen dimension was 100 × 6.5 × 3 mm<sup>3</sup>. UL-94 test was carried out by a Jiangning CFZ-3 instrument (China) according to GB/T2408-2008, and the specimen dimension was 130 × 13 × 3 mm<sup>3</sup>. Cone calorimeter test (CCT) was carried out by an FTT cone calorimeter (UK) at a heat flux of 35 kW m<sup>-2</sup> (ISO 5660, specimen dimension: 100 × 100 × 3 mm<sup>3</sup>). Thermogravimetric analysis (TGA) was conducted

by a TA instruments (America) in the temperature range of 30–800 °C (10 °C min<sup>-1</sup>, N<sub>2</sub> or air atmosphere).

Dynamic mechanical analysis (DMA) was carried out by a TA Q800 analyzer (USA) at a heating rate 3 °C min<sup>-1</sup> in the temperature ranged 30–270 °C, with a frequency of 10 Hz. Tensile strengths of samples were measured by a MTSSANS CMT-5504 electron device (China) according to GB/T 1040–2006, and impact strengths of samples were measured by a MTSSANS E21 pendulum impact machine (China) according to GB/T 1043.1–2008. Every sample was tested in quintuplicate to get the averaged results.

## Results and discussion

### Characterization of CuPB

The micro morphologies of CuPB were observed by TEM, and the elementary composition spectrum is shown in Fig. 1. It can be seen that CuPB agglomerations consist of sphere-like particles with variable diameter size of 200–500 nm, and the particles turn to aggregate. In the spot-scanning EDS spectrum of CuPB, the corresponding elements including C, N, O, P and Cu have been identified.

Figure 2a describes the FTIR spectra of PBA and CuPB. The characterized signals in the FTIR spectrum of PBA including O–H (3100–3000 cm<sup>-1</sup>), C–H (2950 cm<sup>-1</sup> and 1452 cm<sup>-1</sup>), C–N (1161 cm<sup>-1</sup> and 1101 cm<sup>-1</sup>), P=O (1265 cm<sup>-1</sup>), P–O (1033 cm<sup>-1</sup> and 927 cm<sup>-1</sup>) and P–C (759 cm<sup>-1</sup>) have been detected, in agreement with the literatures[34–37]. Compared with the spectrum of PBA, a wide peak around 3200 cm<sup>-1</sup> in the spectrum of CuPB is possibly ascribed to lattice water. Additionally, the XRD spectrum (Fig. 2b) indicates the high crystallization of CuPB.

The surface chemical elements of CuPB were analyzed through XPS, and the related spectra are described in Fig. 2c–e. Elements of Cu, P, N, C and O are confirmed by the survey spectrum of CuPB (Fig. 2c). The peaks located at 931.9 eV and 951.7 eV are attributed to Cu2p<sub>3/2</sub> and Cu2p<sub>1/2</sub>, respectively, with strong shakeup features,

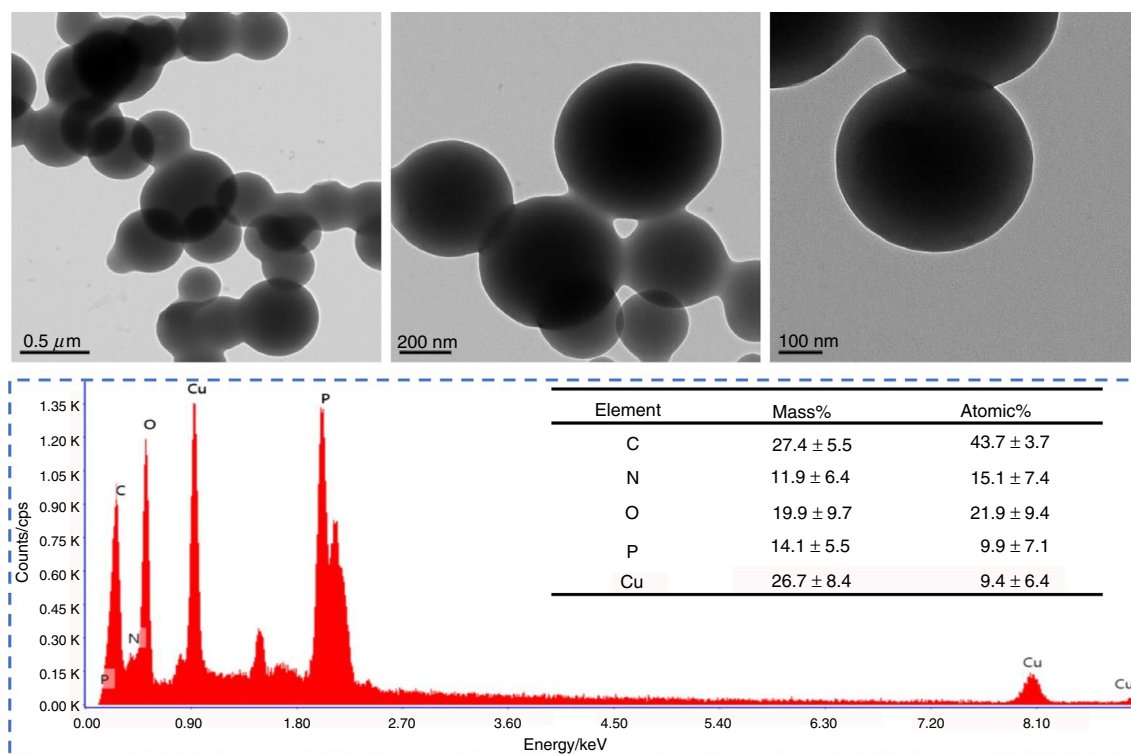


Fig. 1 TEM images and EDS spectrum of CuPB

proving the +2-valence state of Cu ions in CuPB (Fig. 2d) [30]. The peak of P2p is observed at 132.8 eV, indicating the sole state of P in phosphoric acid. The peaks of N1s at 401.0 eV and 399.1 eV correspond to  $\text{NH}^+$  and C–N, respectively (Fig. 2e) [38].

The curves of TG and DTG of CuPB in  $\text{N}_2$  and air atmosphere are depicted in Fig. 2f and the relevant data have been given in Table 2. CuPB exhibits a three-step degradation procedure in  $\text{N}_2$  atmosphere: (i) the removal of lattice water (180–220 °C) [39], (ii) the dehydration and scissions of CuPB chains including C–N and P–C bonds (250–450 °C), (iii) the decompositions of P-containing compounds (> 450 °C)[40]. In comparison, the decomposition of CuPB in air atmosphere is similar to that in  $\text{N}_2$  atmosphere before 150 °C. As the temperature increases, CuPB decomposes earlier in air to produce lattice water. Besides, there is a big mass-loss peak of CuPB in air atmosphere around 500–600 °C, as a result of the oxidation decompositions. However, CuPB shows an increased mass-loss rate around 800 °C in  $\text{N}_2$  atmosphere, which is owing to the transition of copper oxide to cuprous oxide.

## Flame retardancy of EP/CuPB composites

### LOI and UL-94

The flame retardancy performances of pure EP and the flame retarded composites were first assessed by LOI and UL-94. In comparison with the LOI value of pure EP (23.0%), the LOI values of EP/CuPB-1, EP/CuPB-2 and EP/CuPB-3 composites are increased to 26.5%, 28.0% and 28.5%, respectively (Fig. 4a). As seen in the photos of UL-94 test (Fig. 3), only 1.0 mass% CuPB promotes EP material to achieve V-1 rating, compared to the NR (no rating) of pure EP. Moreover, EP containing 2.0 mass% CuPB exhibits a self-extinguish property within less seconds, and 3.0 mass% CuPB promotes EP to achieve V-0 rating, clearly indicative of the high-efficient flame retardancy of CuPB in EP composites.

### CCT

The flame retardancy performances of EP/CuPB composites were overall assessed by CCT, and the results are supplied in Fig. 4 and Table 3. It is found from the results of time to ignition (TTI) that the TTI values of EP/CuPB composites are ca. 10 s ahead of pure EP (Table 3). CuPB on heating

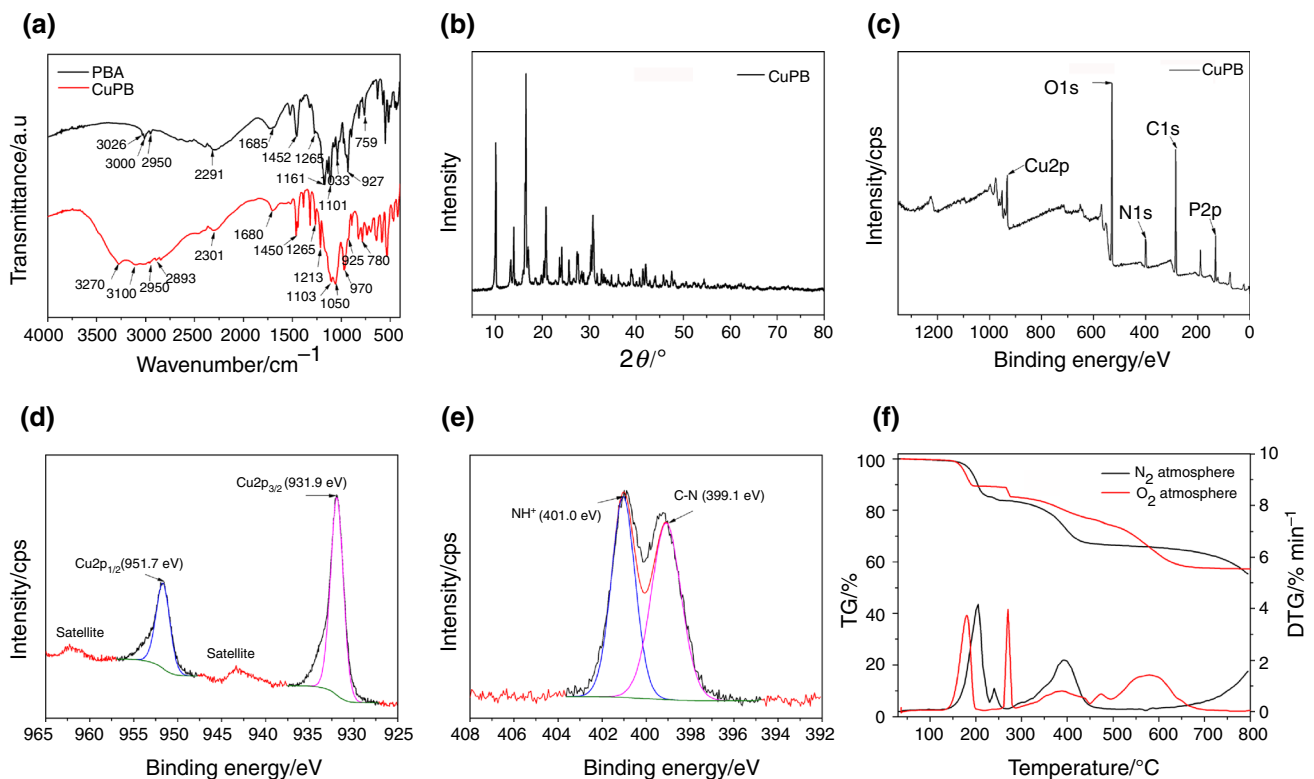


**Fig. 2** **a** FTIR spectra of PBA and CuPB; **b** XRD spectrum of CuPB; **c** XPS survey spectrum of CuPB; **d–e** higher resolution spectra of Cu<sub>2</sub>p and N1s; **f** TG and DTG curves of CuPB

**Table 2** TG and DTG data of CuPB, EP and EP/CuPB composites

Samples	$T_{\text{onset}}/^{\circ}\text{C}$	$T_{\text{max}}/^{\circ}\text{C}$	Deriv. mass at $T_{\text{max}}/\% \text{ min}^{-1}$	Residue at $800^{\circ}\text{C}/\%$	Theoretical residue at $800^{\circ}\text{C}/\%$
CuPB <sub>N<sub>2</sub></sub>	190	205	4.1	55.3	–
CuPB <sub>air</sub>	175	271	3.9	57.3	–
EP	381	414	19.4	13.6	–
EP/CuPB-1	369	397	18.1	19.8	14.0
EP/CuPB-2	353	386	17.0	24.2	14.4
EP/CuPB-3	350	382	16.2	26.8	14.9

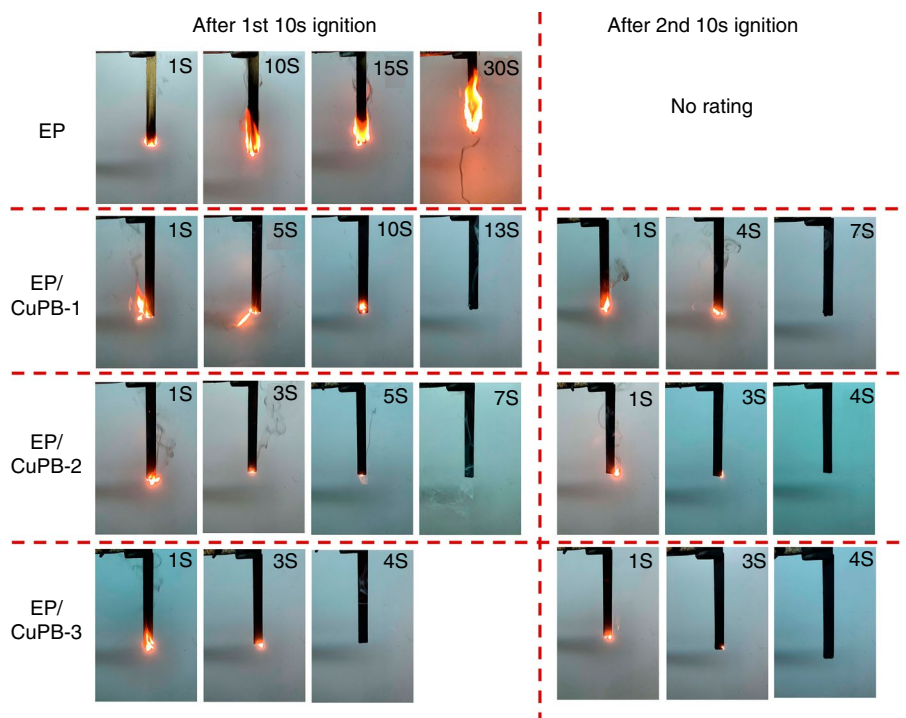
can decompose to release some phosphorus-containing compounds, which may catalyze the decomposition of EP to produce some volatile compounds, resulting in the earlier ignition of EP/CuPB composites [41].

A phenomenon has been observed from Fig. 4b that there is only one peak in the heat release rate (HRR) curve of pure EP, whereas two peaks appear on the HRR curves of EP/CuPB composites, which is probably owing to the secondary decomposition of the char. As the time increases, the pure EP reaches the peak HRR (pHRR) value of  $742 \text{ kW m}^{-2}$ , while the pHRR values of EP/CuPB-1, EP/CuPB-2 and EP/CuPB-3 composites are reduced to  $552 \text{ kW m}^{-2}$ ,  $472 \text{ kW m}^{-2}$  and  $419 \text{ kW m}^{-2}$ , a decrease by 25.6%, 36.4%

and 43.5%, respectively. Additionally, the total heat release (THR) values of EP/CuPB-1, EP/CuPB-2 and EP/CuPB-3 composites are also respectively reduced by 14.0%, 23.7% and 28.0%, in comparison to the values of pure EP (Fig. 4c). The smoke parameters including smoke production rate (SPR) and total smoke release (TSR) are also suppressed (Fig. 4d–e). Compared to that of pure EP, the TSR values of EP/CuPB-1, EP/CuPB-2 and EP/CuPB-3 composites decrease by 28.7%, 35.8% and 37.3%, respectively. Moreover, the peak CO and CO<sub>2</sub> production rates of EP/CuPB composites are gradually reduced with the increased addition of CuPB (Fig. 4f–g). Intriguingly, there is a special phenomenon that the CO production rates of EP/CuPB-1 and EP/



**Fig. 3** UL-94 photos of EP and EP/CuPB composites



CuPB-2 composites have been accelerated after *ca.* 350 s, which is possibly generated from the uncompleted combustion of composites as the result of the weaker barrier effect of the carbon layers. Remarkably, the addition of 3.0 mass% CuPB leads to a 51.9% and 42.0% decrease in the peak CO and CO<sub>2</sub> production rates of the flame retarded EP composite, respectively.

The decreased pHRR, THR, TSR and peak CO production rate of EP/CuPB composites can be explained that CuPB decomposes to deliver some phosphorus-containing acids at low temperatures, promoting the degradation-carbonization process of epoxy. Meanwhile, copper oxides have been demonstrated to improve the structure of the char [42]. The enhanced char residues can retard the thermal and mass exchange between the underlying EP matrix and combustion zone by means of acting as carbon barrier layers, resulting in a lower heat and smoke release.

In order to give a comprehensive evaluation on the fire safety effect of CuPB on EP, the fire performance index (FPI) and fire growth index (FGI) are calculated and presented in Fig. 4h. FPI and FGI correspond to the quotient of TTI divided by pHRR and pHRR divided by the time to pHRR (TTP), respectively [43]. A higher FPI suggests that there is more time available for the rescue before the fire reaches flashover, but a higher FGI indicates that a material is fast ignited to reach a high pHRR [44, 45]. With the incorporation of CuPB into EP, the FPI values are increased but the FGI values are decreased, suggesting the increased fire safety performances of EP.

The mass-loss graphs during the combustion of EP and EP/CuPB composites are depicted in Fig. 4i. Pure EP produces the least char residue after the combustion, and an increase on the yield of the char residues of EP/CuPB composites is obtained proportionally to the CuPB addition, with the sequence of pure EP (10.2%) < EP/CuPB-1 (19.8%) < EP/CuPB-2 (24.0%) < EP/CuPB-3 (26.3%). Moreover, Fig. 5 supplies the digital photos of the char residues of these composites. Clearly, pure EP obtains a fragile and even broken char residue after combustion, indicating the weak charring property. More expandable and loose char residue has been observed for EP/CuPB-1 composite, with large blowholes throughout the char residue, which is possibly resulted by the penetration of inert gases that decomposed from CuPB. With the increase in CuPB to 2.0 mass% and 3.0 mass%, the char residues become denser and more compact with less blowholes on the surface of the char residues. The enhanced char residues present the “tortuous path” effect on inhibiting the thermal and mass exchange of EP/CuPB composites during the combustion, which explains the results in HRR, THR and TSR: If there was more mass remained in the char, there would be less flammable gases and smoke particles in the gas phase [46, 47].

The characterization of the char residues after CCT was performed by the SEM-EDS in Fig. 6. Smooth surface with much gullies is observed from the char residue of pure EP (Fig. 6a), while the char residue from EP/CuPB-2 composite turns to be complete and more delicate (Fig. 6b).

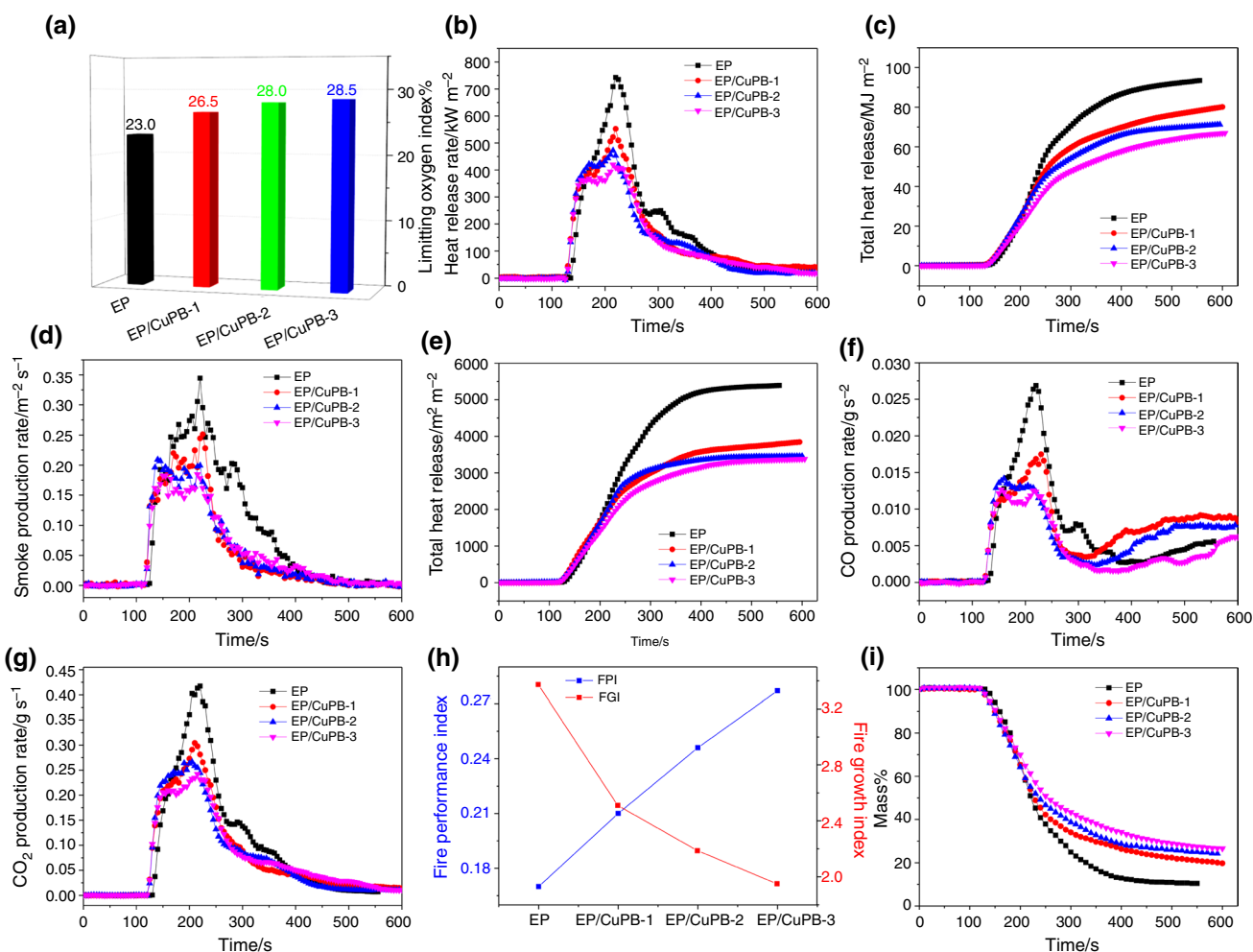


**Fig. 4** a Limiting oxygen index; and curves of **b** heat release rate, **c** total heat release, **d** smoke production rate, **e** total smoke release, **f** CO production rate, **g** CO<sub>2</sub> production rate, **h** fire performance and fire growth index, **i** mass of EP and EP/CuPB composites

**Table 3** Cone calorimeter data of EP and EP/CuPB composites

Samples	TTT <sup>a</sup> /s	pHRR <sup>b</sup> /kW m <sup>-2</sup>	THR <sup>c</sup> /MJ m <sup>-2</sup>	TSR <sup>d</sup> /m <sup>2</sup> m <sup>-2</sup>	Mass <sup>e</sup> /%	FPI <sup>f</sup>	FGI <sup>g</sup>
EP	126 ± 2	742 ± 11	93 ± 1	5390 ± 87	10.2 ± 0.5	0.170 ± 0.005	3.373 ± 0.065
EP/CuPB-1	116 ± 2	552 ± 18	80 ± 2	3842 ± 61	19.8 ± 0.6	0.210 ± 0.011	2.510 ± 0.117
EP/CuPB-2	116 ± 2	472 ± 14	71 ± 2	3459 ± 74	24.0 ± 1.0	0.246 ± 0.012	2.186 ± 0.096
EP/CuPB-3	116 ± 2	419 ± 13	67 ± 3	3379 ± 72	26.3 ± 1.3	0.277 ± 0.014	1.949 ± 0.098

<sup>a</sup>Time to ignition; <sup>b</sup>Peak heat release rate; <sup>c</sup>Total heat release; <sup>d</sup>Total smoke release; <sup>e</sup>Mass of char residues; <sup>f</sup>Fire performance index; <sup>g</sup>Fire growth index

Intriguingly, there are some small pores on the surface of the char residue of EP/CuPB-2 composite, which may result from the penetration of inert gases (e.g., nitrogen-containing gases) that decomposed from CuPB. Compared with the EDS results of pure EP, the percentages of C and O elements are decreased, while the percentages of N, P and Cu elements are increased in the EDS results of the EP/CuPB-2 composite, demonstrating the main flame retardancy of CuPB for EP in the condensed phase. Besides, the

P/Cu atomic ratio in the char residue of EP/CuPB-2 composite is approximately 19:22, which is intermediate between the mole ratio of P/Cu in Cu<sub>3</sub>(PO<sub>4</sub>)<sub>2</sub> (2:3) and Cu<sub>2</sub>P<sub>2</sub>O<sub>7</sub> (1:1), which is further confirmed in the later XRD pattern of the char residues ((Fig. 7b).

FTIR and XRD spectra of the residual chars of EP and EP/CuPB-2 were further collected to reveal the chemical components and structures. The FTIR absorption peaks around 1600 cm<sup>-1</sup> and 1200 cm<sup>-1</sup> are, respectively, ascribed

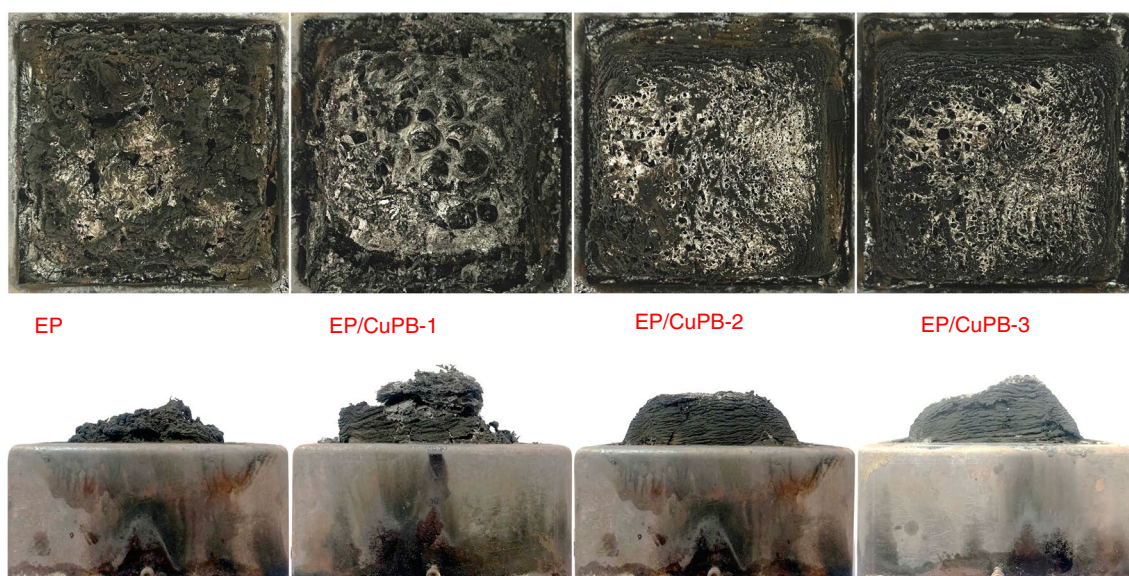


Fig. 5 Digital photographs of the char residues of EP and EP/CuPB composites

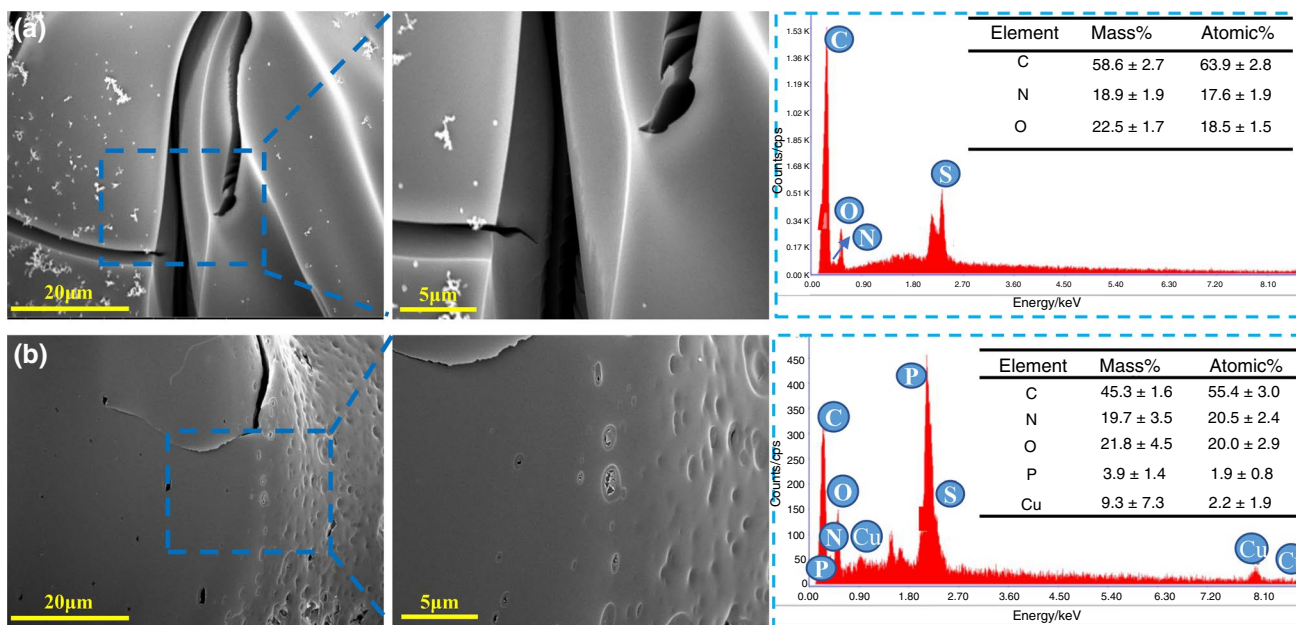


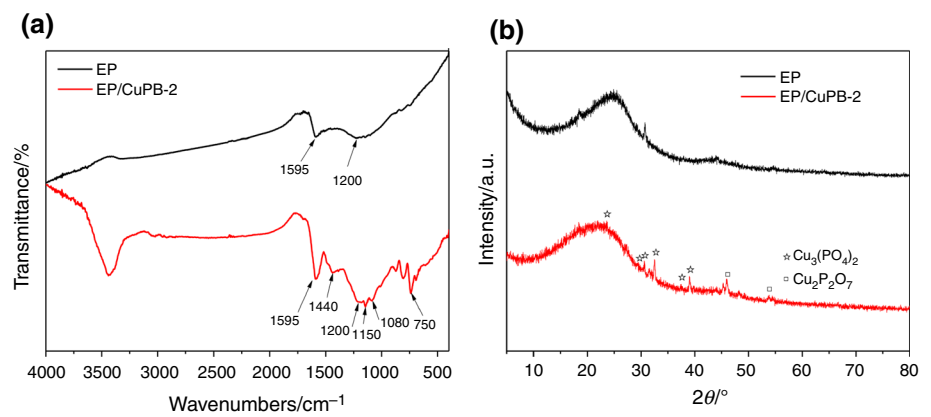
Fig. 6 SEM-EDS of char residues after CCT: **a** EP, **b** EP/CuPB-2

to C=C and C-C groups (Fig. 7a). Besides, there are some additional absorption peaks in the FTIR graph of the residual char of EP/CuPB-2 composite, including P=O groups (around  $1150\text{ cm}^{-1}$ ) and P-O groups (around  $1080\text{ cm}^{-1}$  and  $750\text{ cm}^{-1}$ ) [48]. Pure EP displays an amorphous char residue from the XRD results, but some crystalline signals have been identified in the char residue of EP/CuPB-2 composite, which are attributed to the patterns of  $\text{Cu}_3(\text{PO}_4)_2$  and  $\text{Cu}_2\text{P}_2\text{O}_7$  (Fig. 7b). The above results reveal that some

phosphorus-containing compounds are retained in the chars of EP/CuPB composites, indicating the formation of some intermediates such as phosphoric or metaphosphoric acids during the combustion of composites.

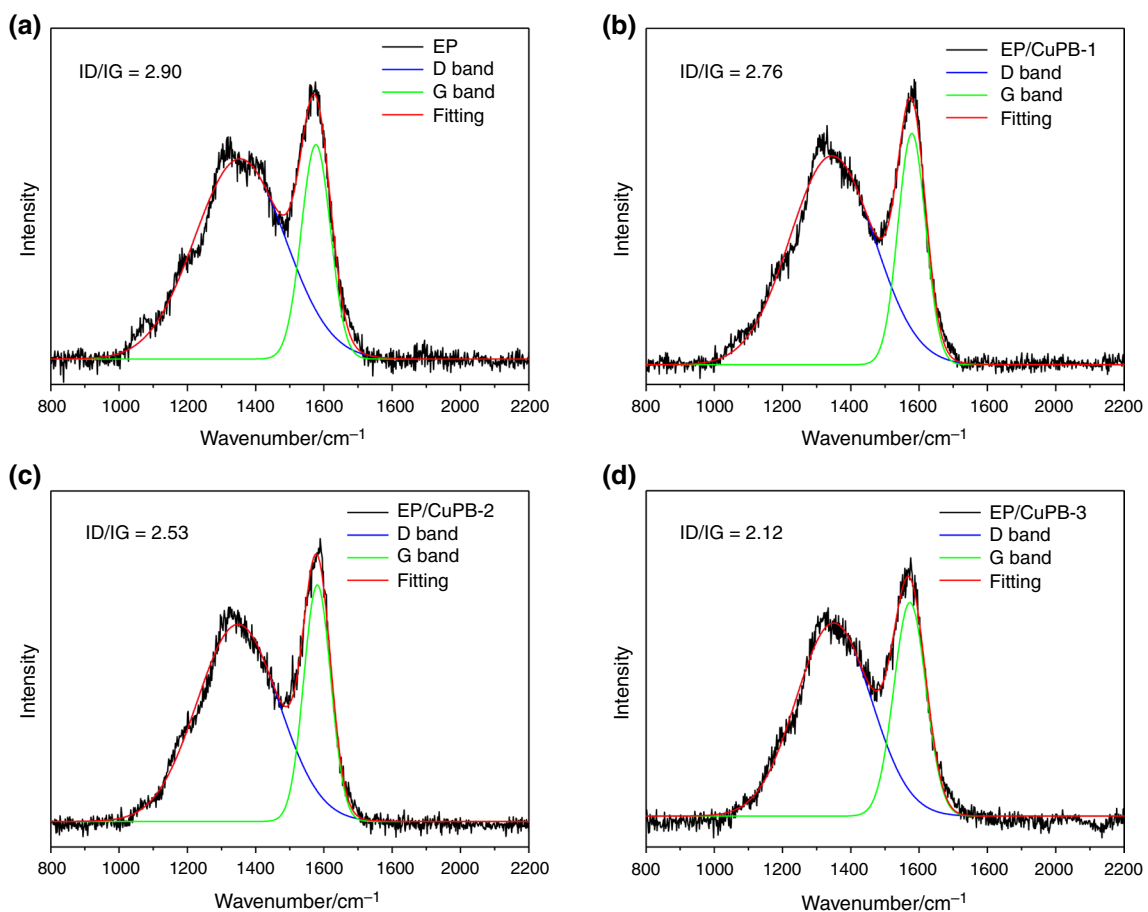
Raman spectra were also utilized to characterize the graphitization degree of the residual chars of EP and EP/CuPB composites. The respective spectra are shown in Fig. 8a-d. There are two bands appearing at  $1350\text{ cm}^{-1}$  (D band) and  $1560\text{ cm}^{-1}$  (G band), which is, respectively, assigned to the



**Fig. 7** **a** FTIR and **b** XRD spectra of char residues after CCT

vibrations of amorphous carbons and crystalline graphite [49, 50]. The integrated intensity ratio of ID to IG (ID/IG) is applied to evaluate the graphitization degree of the char, and the higher ID/IG represents the char with the lower graphitization degree [51]. The ID/IG values of EP and EP/CuPB composites are calculated and ranged in the following order: EP (2.90) > EP/CuPB-1 (2.76) > EP/CuPB-2 (2.53) > EP/CuPB-3 (2.12). The highest ID/IG value of the

char residue of pure EP indicates the fragile char with the lowest graphitization degree, which is insufficient to prevent the thermal and mass exchange between the condense and gaseous phase. The incorporation of CuPB decreases the ID/IG values of the char residues, demonstrating the improved graphitization degree of the char residues, resulting in better shielding effect between the underlying matrix and combustion zone.

**Fig. 8** Raman spectra of the char residues of **a** EP, **b** EP/CuPB-1, **c** EP/CuPB-2, **d** EP/CuPB-3

Based on above results, the flame-retardant mechanism of CuPB in EP is tentatively proposed (Fig. 9). At the beginning of the combustion of EP/CuPB composites, CuPB decomposes to produce some phosphorus-containing compounds (e.g., phosphoric or metaphosphoric acids) with strong dehydration property and catalysis in enhancing the char-forming process of epoxy to form dense chars [52]. Meanwhile, the copper-containing compounds further improve the structure of the chars [42]. The robust char residues acting as physical barriers are regarded as beneficial in thermal insulation as well as preventing the mass exchange between the underlying matrix with combustion zone. Besides, CuPB as a nitrogen-containing compound may release some volatile nitrogen-containing inert gases, which works in the flame (Fig. 5) [32, 53].

### Thermal decomposition of EP/CuPB composites

Figure 10 displays the TG and DTG curves of EP and EP/CuPB composites, and some characteristic parameters are recorded in Table 2. Pure EP has only one considerable decomposition step in the range of 300–500 °C, which corresponds to the decomposition of the backbones of EP matrix [54]. The incorporation of CuPB has less effect on the decomposition steps of EP for the marginal loading of CuPB and the overlapped degradation process. The temperatures at 5.0 mass% mass loss ( $T_{\text{onset}}$ ) of pure EP occur at 381 °C, which is higher than those of EP/CuPB composites (369 °C, 353 °C and 350 °C of EP/CuPB-1, EP/CuPB-2 and EP/CuPB-3, respectively). The lower  $T_{\text{onset}}$  corresponds to the early decomposition of CuPB and the

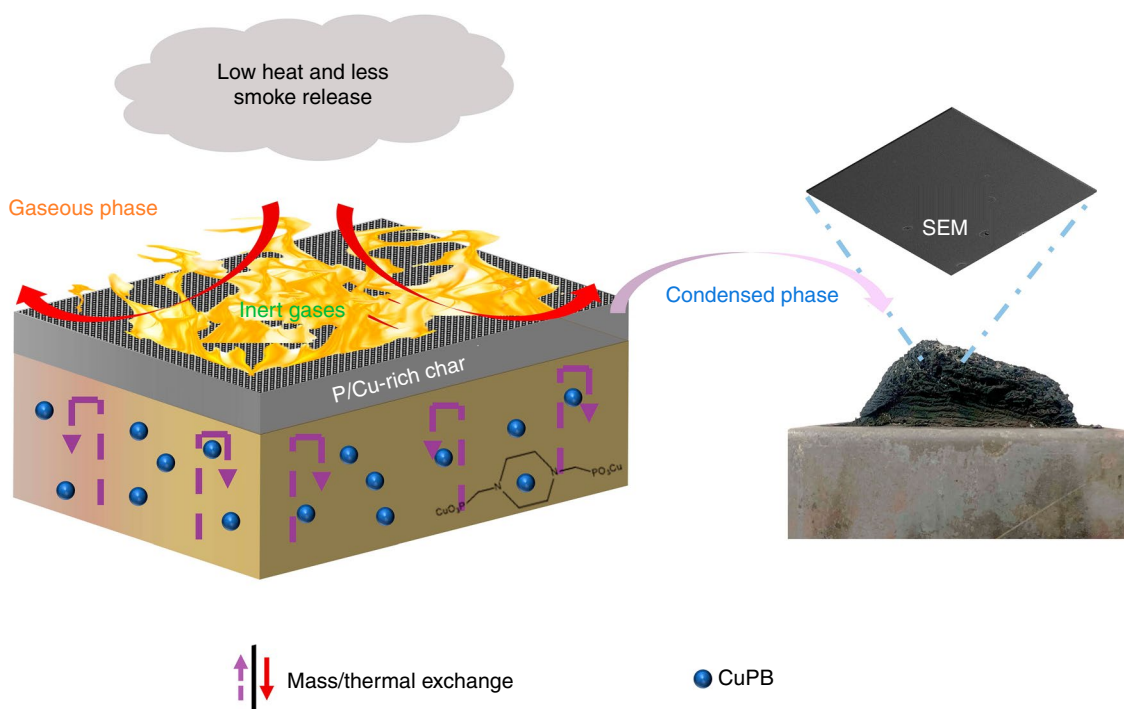
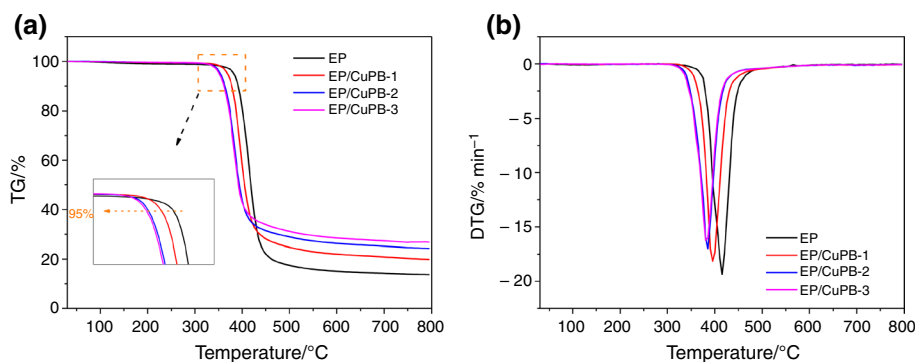


Fig. 9 The proposed flame-retardant mechanism of CuPB in EP

Fig. 10 TG **a** and DTG **b** curves of EP and EP/CuPB composites



catalyzed degradation of EP matrix by CuPB. Additionally, the  $T_{\max}$  (temperature at the maximum mass loss rate) values of EP/CuPB-1, EP/CuPB-2 and EP/CuPB-3 composites are also reduced, but the maximum mass loss rates decrease to  $18.1\% \text{ min}^{-1}$ ,  $16.8\% \text{ min}^{-1}$  and  $16.2\% \text{ min}^{-1}$ , respectively, in comparison with that of pure EP ( $19.4\% \text{ min}^{-1}$ ). There is only 13.6% char residue left of pure EP at  $800\text{ }^\circ\text{C}$ , while the char residues of the flame retarded EP/CuPB-1, EP/CuPB-2 and EP/CuPB-3 composites reach up to 19.8%, 24.2% and 24.4%, respectively. According to the literature [55], the theoretical char residues of EP/CuPB composites have been calculated (Table 2). Significant increase in the real char residues of EP/CuPB composites has been observed compared with the theoretical residues, which illustrates the promoting carbonization function of CuPB in EP. It is reported that the earlier thermal decomposition and higher volatility of metallic phosphonates play an important role in the gas phase by

flame suppression [56, 57]. Besides, owing to the famous char-forming function of phosphorus-containing compounds and the improvement on the char residue of copper-containing compounds [42], the good carbonization of CuPB in EP is promoted and the char residues are enhanced.

TG-IR combination was conducted to analyze the pyrolysis compounds from EP and EP/CuPB-2 composites. In the spectra of pure EP (Fig. 11a), no other absorption peaks of the pyrolysis compounds from EP appear obviously at  $200\text{ }^\circ\text{C}$ , except  $\text{CO}_2$  (around  $2350\text{ cm}^{-1}$ ) which is owing to the background disturbances. As the temperature further increases, some volatile ether components ( $1240\text{--}1130\text{ cm}^{-1}$ ), aromatic compounds ( $1514\text{ cm}^{-1}$ ,  $1400\text{--}1300\text{ cm}^{-1}$ ) [58],  $\text{C}=\text{O}$  compounds ( $1750\text{--}1640\text{ cm}^{-1}$ ) [22],  $\text{CO}$  (around  $2170\text{ cm}^{-1}$ ) [59], hydrocarbon components (around  $3010\text{ cm}^{-1}$  and  $2960\text{ cm}^{-1}$ ), nitrogenous components (around  $3400\text{ cm}^{-1}$ ), and  $\text{--OH}$

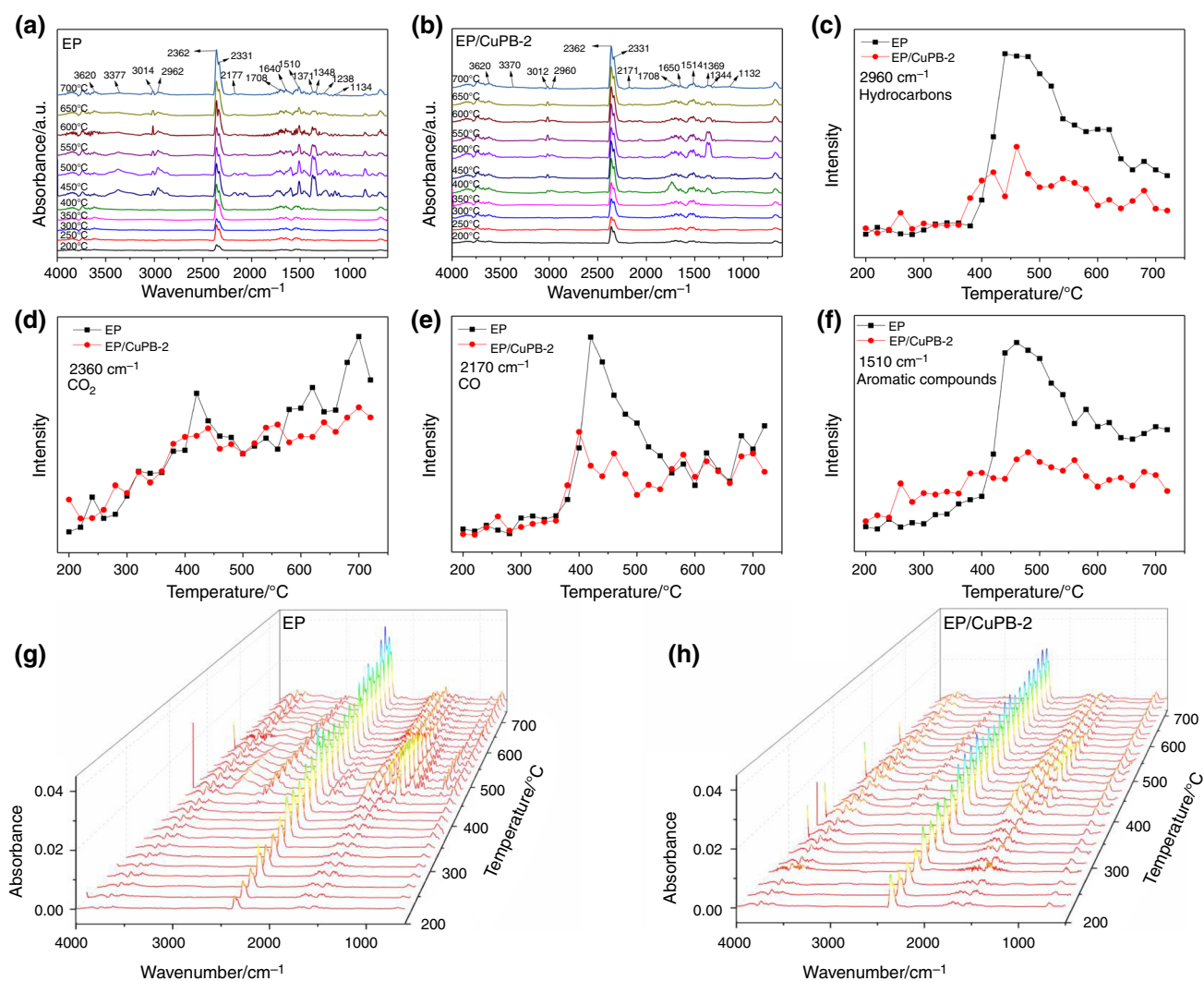


**Fig. 11** Absorbance of pyrolysis products of **a** EP and **b** EP/CuPB-2 at different temperatures; absorbance of **c** hydrocarbons, **d**  $\text{CO}_2$ , **e**  $\text{CO}$ , **f** aromatic compounds for EP and EP/CuPB-2; 3D TG-FTIR spectra of **g** EP and **h** EP/CuPB-2

compounds (around  $3600\text{ cm}^{-1}$ ) have been detected. There is a huge increase on the peak intensities of pure EP at about  $450\text{ }^{\circ}\text{C}$ , while EP/CuPB-2 composite decreases this temperature to about  $400\text{ }^{\circ}\text{C}$  (Fig. 11b), in agreement with the premature degradation temperatures of EP/CuPB composites in TG analysis. The changes can also be observed from that there are slight movements in the relative intensities of some pyrolysis compounds (e.g., hydrocarbon,  $\text{CO}_2$ , CO and aromatic components) of EP/CuPB-2 composite between  $400\text{--}450\text{ }^{\circ}\text{C}$ , contrasted with the sharp increase on the relative intensities of these compounds of pure EP (Fig. 11c–f). In the temperature range of  $400\text{--}700\text{ }^{\circ}\text{C}$ , the relative intensities of hydrocarbon, CO and aromatic components of EP/CuPB-2 composite are much suppressed compared with that of pure EP. The results can be explained that CuPB has decomposed into some phosphoric or metaphosphoric acids at low temperature to promote the char-forming process of EP/CuPB composites. The dense char residues exhibit better thermal stability and display excellent “tortuous path” effect on inhibiting the thermal and mass exchange, reducing the release of volatile gases including C-H and aromatic compounds, which act as fuels and aggregate to produce harmful smokes, respectively [60].

## Mechanical properties of EP/CuPB composites

DMA test was carried out to measure the thermal–mechanical behaviors of EP/CuPB composites, and the results of storage modulus ( $E'$ ) and Tan delta are demonstrated in Fig. 12a–b. The  $E'$  of pure EP gradually decreases along with the temperature, indicating the increased elasticity of the molecular chains of EP at high temperatures [61]. Similarly, the tendency of  $E'$  has not been much changed with the introduction of CuPB, but the initial  $E'$  values of EP/CuPB composites show a little increase compared with that of pure EP, especially for EP/CuPB-2 composite. It is known that the higher  $E'$  requires more energy for polymer chains to move, and the increased  $E'$  of EP/CuPB-2 composites supports the reinforced rigidity of EP/CuPB composites which suggests that the high rigidity of CuPB block the movement of the molecular chains of EP [62]. The tan delta peaks of EP/CuPB composites are significantly suppressed, and the glass transition temperature ( $T_g$ , the temperature assigned to peak tan delta) is slightly increased in comparison with that of pure EP, with an increase by  $3\text{ }^{\circ}\text{C}$ ,  $6\text{ }^{\circ}\text{C}$  and  $7\text{ }^{\circ}\text{C}$  for EP/CuPB-1, EP/CuPB-2 and EP/CuPB-3 composite, respectively. The increased  $T_g$  indicates that CuPB particles delay the transition of epoxy from high elastic state to glassy state, by means of hindering the movement of the molecular chains of EP. Hence, it can be concluded that EP/CuPB composites still possess higher thermal–mechanical performances at high temperatures.

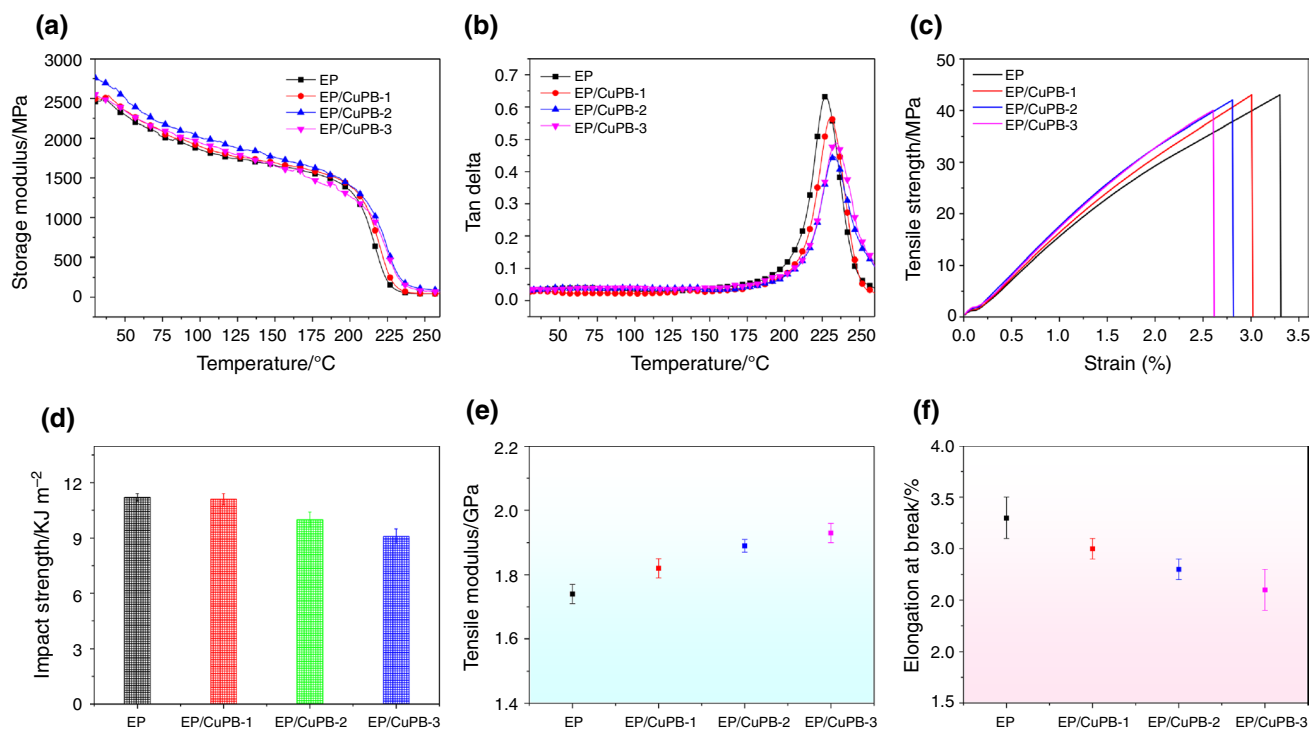
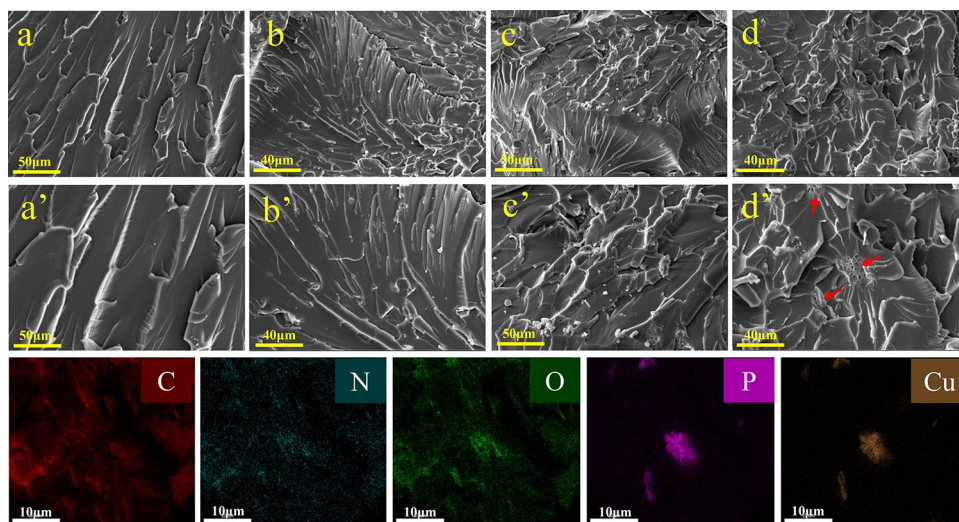


**Fig. 12** a Storage modulus, b tan delta, c tensile strength, d impact strength, e tensile modulus and f elongations at breaks of EP and EP/CuPB composites



**Fig. 13** SEM images at different magnifications of fractures after tensile test of (a, a') EP; (b, b') EP/CuPB-1, (c, c') EP/CuPB-2, (d, d') EP/CuPB-3; and the elemental mapping images of (d')



Moreover, the effect of CuPB on the mechanical properties (tensile and impact strengths, elongation at break and tensile modulus) of EP nanocomposites was further investigated, and the relevant data are summarized in Fig. 12c–f. The tensile and impact strengths of pure EP are 43 and 11.2 MPa, respectively. After the incorporation of 1.0 mass% CuPB to EP, the tensile and impact strengths of composite are almost not affected in comparison with that of pure EP, indicating the good compatibility between CuPB particles and epoxy. When the loading of CuPB rises to 2.0 mass%, a slight decrease in the tensile and impact strength of the flame retarded EP composite has been observed. Compared the values of pure EP, the tensile and impact strengths of EP/CuPB-3 composite decrease by 7.0% and 18.7%, respectively (Fig. 12c–d). In addition, the elongation at break and tensile modulus of pure EP is 3.3% and 1.74 GPa, respectively. By comparison, the introduction of 3.0 mass% CuPB decreases the elongation at break of EP by 21.2%, and increases the tensile modulus by 10.9% (Fig. 12e–f). This suggests that CuPB can improve the deformation resistance of EP, owing to the fact that CuPB hinders the movement of EP chains. However, on the other hand, the blocking effect of CuPB decreases the flexibility of polymer chains, leading to a decreased elasticity of EP [32]. The results meet well with that in the DMA test.

As reported, the mechanical performances of polymeric composites are usually affected by the dispersion of additives and the interfacial interaction between additives and polymers matrix [63]. In order to explore the dispersion of CuPB in EP, SEM was applied to investigate the morphologies of the tensile fractures of EP and EP/CuPB composites. As shown in Fig. 13a, a', the fracture surface of pure EP exhibits smooth and regular traces, illustrating the brittle rupture. The fracture surface of EP/CuPB-1 composite has not been much changed with much wrinkles (Fig. 13b, b'). Some tortuous and irregular traces criss-cross mingle on the fracture surfaces of EP/CuPB-2

and EP/CuPB-3 composites (Fig. 13c–d). At 3.0 mass% CuPB loading, there are some aggregations of the nano particles on the fracture surface of EP/CuPB-3 composite, which may be due to the strong van der Waals forces between the nano particles (Fig. 13d'). It is further confirmed in the element mapping images of the fracture of EP/CuPB-3 composites, with the partial aggregations of Cu and P. The aggregation of CuPB may result in some defects inside EP matrix, leading to partial stress concentrations under external force [48]. In general, CuPB as a metal–organic phosphonate possesses relatively good compatibility with EP, and the nano particles are well dispersed into EP matrix. Therefore, CuPB shows less mechanical influence on EP, which is acceptable for most applications of EP.

## Conclusions

A metal–organic phosphonate (CuPB) was synthesized and used to modify EP, the flame retardancy, thermal decomposition and mechanical properties of EP/CuPB composites are studied. The results of TEM, FTIR and XPS confirm the successful synthesis of CuPB. UL-94 result shows that only 3.0 mass% CuPB promotes EP to achieve UL-94 V-0 grade. CCT results reveal that the pHRR, THR and TSR values are remarkably suppressed by the introduction of CuPB to EP. TG and TG-IR results demonstrate that the incorporation of CuPB increases the char residues and suppresses the emission of volatile compounds (e.g., aromatic compounds) during the thermal decomposition of EP. Moreover, CuPB slightly improves the T<sub>g</sub> of EP and has less influence on the mechanical properties of EP. It has provided a new strategy to improve the fire safety performances of EP meanwhile maintain its thermal and mechanical properties.

**Acknowledgements** This work was financially supported by the National Natural Science Foundation of China (21975185).

**Funding** This work was financially supported by the National Natural Science Foundation of China (21975185).

### Compliance with ethical standards

**Conflicts of interest** The authors declare that there is no conflict of interests regarding the publication of this article.

### References

- Jiang S, Tang G, Chen J, Huang Z, Hu Y. Biobased polyelectrolyte multilayer-coated hollow mesoporous silica as a green flame retardant for epoxy resin. *J Hazard Mater*. 2018;342:689–97.
- Hu X, Yang H, Jiang Y, He H, Liu H, Huang H, et al. Facile synthesis of a novel transparent hyperbranched phosphorous/nitrogen-containing flame retardant and its application in reducing the fire hazard of epoxy resin. *J Hazard Mater*. 2019;379:120793.
- Luo Q, Yuan Y, Dong C, Huang H, Liu S, Zhao J. Highly effective flame retardancy of a novel DPPA-based curing agent for DGEBA epoxy resin. *Ind Eng Chem Res*. 2016;55(41):10880–8.
- Yang G, Wu W, Wang Y, Jiao Y, Lu L, Qu H, et al. Synthesis of a novel phosphazene-based flame retardant with active amine groups and its application in reducing the fire hazard of Epoxy Resin. *J Hazard Mater*. 2019;366:78–87.
- Luo QQ, Sun YL, Yu B, Li CP, Song JL, Tan DX, et al. Synthesis of a novel reactive type flame retardant composed of phenophosphazine ring and maleimide for epoxy resin. *Polym Degrad Stab*. 2019;165:137–44.
- Tamura K, Ohyama S, Umeyama K, Kitazawa T, Yamagishi A. Preparation and properties of halogen-free flame-retardant layered silicate-polyamide 66 nanocomposites. *Appl Clay Sci*. 2016;126:107–12.
- Rakotomalala M, Wagner S, Doring M. Recent Developments in halogen free flame retardants for epoxy resins for electrical and electronic applications. *Materials*. 2010;3(8):4300–27.
- Tan Y, Shao Z, Chen X, Long J, Chen L, Wang Y. Novel multifunctional organic–inorganic hybrid curing agent with high flame-retardant efficiency for epoxy resin. *ACS Appl Mater Inter*. 2015;7(32):17919–28.
- Qiu Y, Liu Z, Qian L, Hao J. Pyrolysis and flame retardant behavior of a novel compound with multiple phosphaphenanthrene groups in epoxy thermosets. *J Anal Appl Pyrolysis*. 2017;127:23–30.
- Sudhakara P, Kannan P, Obireddy K, Varada RA. Organophosphorus and DGEBA resins containing clay nanocomposites: flame retardant, thermal, and mechanical properties. *J Mater Sci*. 2011;46(8):2778–88.
- Wang X, Hu Y, Song L, Yang H, Xing W, Lu H. Synthesis and characterization of a DOPO-substituted organophosphorus oligomer and its application in flame retardant epoxy resins. *Prog Org Coat*. 2011;71(1):72–82.
- Ma S, Liu X, Jiang Y, Fan L, Feng J, Zhu J. Synthesis and properties of phosphorus-containing bio-based epoxy resin from itaconic acid. *Sci China Chem*. 2014;57(3):379–88.
- Wang C, Shieh J. Phosphorus-containing epoxy resin for an electronic application. *J Appl Polym Sci*. 2015;73(3):353–61.
- Yang S, Wang J, Huo S, Cheng L, Wang M. Preparation and flame retardancy of an intumescent flame-retardant epoxy resin system constructed by multiple flame-retardant compositions containing phosphorus and nitrogen heterocycle. *Polym Degrad Stab*. 2015;119:251–9.
- Zhang Y, Yu B, Wang B, Liew KM, Song L, Wang C, et al. Highly Effective P-P Synergy of a Novel DOPO-Based Flame Retardant for Epoxy Resin. *Ind Eng Chem Res*. 2017;56(5):1245–55.
- Chi Z, Guo Z, Xu Z, Zhang M, Li M, Shang L, et al. A DOPO-based phosphorus-nitrogen flame retardant bio-based epoxy resin from diphenolic acid: synthesis, flame-retardant behavior and mechanism. *Polym Degrad Stab*. 2020;176:109151.
- Jin E, Chung Y. Combustion characteristics of *Pinus rigida* specimens treated with mixed phosphorus-nitrogen additives. *J Ind Eng Chem*. 2016;36:74–9.
- Feng YZ, He CG, Wen YF, Ye YS, Zhou XP, Xie XL, et al. Superior flame retardancy and smoke suppression of epoxy-based composites with phosphorus/nitrogen co-doped graphene. *J Hazard Mater*. 2018;346:140–51.
- Li A, Mao P, Liang B. The effect of a novel phosphorus-nitrogen reactive flame retardant curing agent on the performance of epoxy resin. *J Macromol Sci A*. 2019;56:1–10.
- Liu L, Zhang Y, Li L, Wang Z. Microencapsulated ammonium polyphosphate with epoxy resin shell: preparation, characterization, and application in EP system. *Polym Adv Technol*. 2011;22(12):2403–8.
- Zhu Z, Wang L, Dong L. Influence of a novel P/N-containing oligomer on flame retardancy and thermal degradation of intumescent flame-retardant epoxy resin. *Polym Degrad Stab*. 2019;162:129–37.
- Liu L, Xu Y, Xu M, Li Z, Hu Y, Li B. Economical and facile synthesis of a highly efficient flame retardant for simultaneous improvement of fire retardancy, smoke suppression and moisture resistance of epoxy resins. *Compos Part B Eng*. 2019;167:422–33.
- Sun Z, Hou Y, Hu Y, Hu W. Effect of additive phosphorus-nitrogen containing flame retardant on char formation and flame retardancy of epoxy resin. *Mater Chem Phys*. 2018;214:154–64.
- Liu Y, Cao Z, Zhang Y, Fang Z. Synthesis of Cerium N-Morpholinomethylphosphonic Acid and Its Flame Retardant Application in High Density Polyethylene. *Ind Eng Chem Res*. 2013;52(15):5334–40.
- Cai Y, Guo Z, Fang Z, Cao Z. Effects of layered lanthanum phenylphosphonate on flame retardancy of glass-fiber reinforced poly(ethylene terephthalate) nanocomposites. *Appl Clay Sci*. 2013;77–78:10–7.
- Hou Y, Hu W, Gui Z, Hu Y. A novel Co(II)-based metal-organic framework with phosphorus-containing structure: Build for enhancing fire safety of epoxy. *Composites Sci Technol*. 2017;152:231–42.
- Hou Y, Hu W, Gui Z, Hu Y. Preparation of metal-organic frameworks and their application as flame retardants for polystyrene. *Ind Eng Chem Res*. 2017;56(8):2036–45.
- Wang J, Qian L, Xu B, Xi W, Liu X. Synthesis and characterization of aluminum poly-hexamethylenephosphinate and its flame-retardant application in epoxy resin. *Polym Degrad Stab*. 2015;122:8–17.
- Ma S, Hou Y, Xiao Y, Chu F, Cai T, Hu W, et al. Metal-organic framework@polyaniline nanoarchitecture for improved fire safety and mechanical performance of epoxy resin. *Mater Chem Phys*. 2020;247:122875.
- Wang J, Yuan B, Mu X, Feng X, Tai Q, Hu Y. Two-dimensional metal phenylphosphonates as novel flame retardants for polystyrene. *Ind Eng Chem Res*. 2017;56(25):7192–206.
- Zhou T, Wu T, Xiang H, Li Z, Xu Z, Kong Q, et al. Simultaneously improving flame retardancy and dynamic mechanical properties of epoxy resin nanocomposites through synergistic effect of zirconium phenylphosphate and POSS. *J Therm Anal Calorim*. 2019;135(4):2117–24.

32. Zhu M, Liu L, Wang Z. Mesoporous silica via self-assembly of nano zinc amino-tris-(methylenephosphonate) exhibiting reduced fire hazards and improved impact toughness in epoxy resin. *J Hazard Mater.* 2020;392:122343.
33. Groves JA, Wright PA, Lightfoot P. Two closely related lanthanum phosphonate frameworks formed by anion-directed linking of inorganic chains. *Inorg Chem.* 2005;44(6):1736–9.
34. Alhendawi H, Brunet E, Payán ER, Shurrab N, Juanes O, Idhair S, et al. A new layered zirconium biphosphonate framework covalently pillared with N, N'-piperazinebis(methylene) moiety: synthesis and characterization. *J Porous Mater.* 2013;20(5):1189–94.
35. Farrokhi A, Jafarpour M, Najafzade R. Phosphonate-based Metal Organic Frameworks as Robust Heterogeneous Catalysts for TBHP Oxidation of Benzylic Alcohols. *Catal Lett.* 2017;147(7):1714–21.
36. Rao W, Liao W, Wang H, Zhao H, Wang Y. Flame-retardant and smoke-suppressant flexible polyurethane foams based on reactive phosphorus-containing polyol and expandable graphite. *J Hazard Mater.* 2018;360:651–60.
37. Villemain D, Moreau B, Elbilali A, Didi M-A, Kaid Mh, Jaffrès P-A. Green Synthesis of Poly(aminomethylenephosphonic) Acids. Phosphorus, Sulfur, and Silicon and the Related Elements. 2010;185(12):2511–9.
38. Cai W, Wang J, Pan Y, Guo W, Mu X, Feng X, et al. Mussel-inspired functionalization of electrochemically exfoliated graphene: Based on self-polymerization of dopamine and its suppression effect on the fire hazards and smoke toxicity of thermoplastic polyurethane. *J Hazard Mater.* 2018;352:57–69.
39. Serre C, Groves JA, Lightfoot P, Slawin AMZ, Wright PA, Stock N, et al. Synthesis, Structure and Properties of Related Microporous N, N'-Piperazinebismethylenephosphonates of Aluminum and Titanium. *Chem Mater.* 2006;18(6):1451–7.
40. Hayashi H, Hudson M. Reaction of the phenylphosphonate anion with the layered basic copper(II) nitrate [Cu<sub>2</sub>(OH)<sub>3</sub>NO<sub>3</sub>]. *J Mater Chem.* 1995;5:115–9.
41. Chen X, Zhang X, Wang W, Wang Y, Jiao C. Fire-safe agent integrated with oyster shell and melamine polyphosphate for thermoplastic polyurethane. *Polym Adv Technol.* 2019;30(7):1576–88.
42. Wang W, Chen X, Gu Y, Jiao C. Synergistic fire safety effect between nano-CuO and ammonium polyphosphate in thermoplastic polyurethane elastomer. *J Therm Anal Calorim.* 2018;131(3):3175–83.
43. Chen X, Wang W, Li S, Jiao C. Fire safety improvement of para-aramid fiber in thermoplastic polyurethane elastomer. *J Hazard Mater.* 2017;324(Part B):789–96.
44. Cross MS, Cusack PA, Hornsby PR. Effects of tin additives on the flammability and smoke emission characteristics of halogen-free ethylene-vinyl acetate copolymer. *Polym Degrad Stab.* 2003;79(2):309–18.
45. Nazaré S, Kandola B, Horrocks AR. Use of cone calorimetry to quantify the burning hazard of apparel fabrics. *Fire Mater.* 2002;26(4–5):191–9.
46. Chen X, Wang W, Jiao C. A recycled environmental friendly flame retardant by modifying para-aramid fiber with phosphorus acid for thermoplastic polyurethane elastomer. *J Hazard Mater.* 2017;331:257–64.
47. Chen X, Wang W, Jiao C. para-Aramid fiber modified by melamine polyphosphate and its flame retardancy on thermoplastic polyurethane elastomer. *Rsc Adv.* 2017;7(84):53172–80.
48. Wang W, Wang Z. Epoxy resin/tin ethylenediamine tetra-methylene phosphonate composites with simultaneous improvement of flame retardancy and smoke suppression. *Polym Adv Technol.* 2020;31(11):2775–88.
49. Cai W, Feng X, Wang B, Hu W, Yuan B, Hong N, et al. A novel strategy to simultaneously electrochemically prepare and functionalize graphene with a multifunctional flame retardant. *Chem Eng J.* 2017;316:514–24.
50. Ferrari AC, Basko DM. Raman spectroscopy as a versatile tool for studying the properties of graphene. *Nat Nanotechnol.* 2013;8(4):235–46.
51. Wang J, Zhang D, Zhang Y, Cai W, Yao C, Hu Y, et al. Construction of multifunctional boron nitride nanosheet towards reducing toxic volatiles (CO and HCN) generation and fire hazard of thermoplastic polyurethane. *J Hazard Mater.* 2019;362:482–94.
52. Kong Q, Wu T, Zhang J, Wang D. Simultaneously improving flame retardancy and dynamic mechanical properties of epoxy resin nanocomposites through layered copper phenylphosphate. *Compos Sci Technol.* 2018;154:136–44.
53. Liu L, Wang Z. Facile synthesis of a novel magnesium amino-tris-(methylenephosphonate)-reduced graphene oxide hybrid and its high performance in mechanical strength, thermal stability, smoke suppression and flame retardancy in phenolic foam. *J Hazard Mater.* 2018;357:89–99.
54. Feng Y, Hu J, Xue Y, He C, Zhou X, Xie X, et al. Simultaneous improvement in the flame resistance and thermal conductivity of epoxy/Al<sub>2</sub>O<sub>3</sub> composites by incorporating polymeric flame retardant-functionalized graphene. *J Mater Chem A.* 2017;5(26):13544–56.
55. Xu Z, Deng N, Yan L, Chu Z. Functionalized multiwalled carbon nanotubes with monocomponent intumescent flame retardant for reducing the flammability and smoke emission characteristics of epoxy resins. *Polym Adv Technol.* 2018;29(12):3002–13.
56. Costes L, Laoutid F, Dumazert L, Lopez-cuesta J-M, Brohez S, Delvosalle C, et al. Metallic phytates as efficient bio-based phosphorus flame retardant additives for poly(lactic acid). *Polym Degrad Stab.* 2015;119:217–27.
57. Braun U, Schartel B. Flame Retardancy Mechanisms of Aluminium Phosphinate in Combination with Melamine Cyanurate in Glass-Fibre-Reinforced Poly(1,4-butylene terephthalate). *Macromol Mater Eng.* 2008;293(3):206–17.
58. Xu Y, Chen L, Rao W, Qi M, Guo D, Liao W, et al. Latent curing epoxy system with excellent thermal stability, flame retardance and dielectric property. *Chem Eng J.* 2018;347:223–32.
59. Chen X, Wang W, Jiao C. In situ synthesis of flame retardant organic-inorganic hybrids by molten blending method based on thermoplastic polyurethane elastomer and polybutyl titanate. *Rsc Adv.* 2016;6(95):92276–84.
60. Feng Y, Wang B, Wang F, Zhao Y, Liu C, Chen J, et al. Thermal degradation mechanism and kinetics of polycarbonate/silica nanocomposites. *Polym Degrad Stab.* 2014;107:129–38.
61. Wan J, Gan B, Li C, Molina-Aldareguia J, Li Z, Wang X, et al. A novel biobased epoxy resin with high mechanical stiffness and low flammability: synthesis, characterization and properties. *J Mater Chem A.* 2015;3(43):21907–21.
62. Fang F, Ran S, Fang Z, Song P, Wang H. Improved flame resistance and thermo-mechanical properties of epoxy resin nanocomposites from functionalized graphene oxide via self-assembly in water. *Compos Part B Eng.* 2019;165:406–16.
63. Jiao J, Sun X, Pinnavaia TJ. Reinforcement of a Rubbery Epoxy Polymer by Mesostructured Silica and Organosilica with Wormhole Framework Structures. *Adv Funct Mater.* 2008;18(7):1067–74.

**Publisher's Note** Springer Nature remains neutral with regard to jurisdictional claims in published maps and institutional affiliations.